

High angular momentum hot differentially rotating equilibrium star evolutions in conformally flat spacetime

Patrick Chi-Kit Cheong^{1,2,*}, Nishad Muhammed³, Pavan Chawhan³, Matthew D. Duez³, Francois Foucart¹, Lawrence E. Kidder⁴, Harald P. Pfeiffer⁵, and Mark A. Scheel⁶

¹*Department of Physics and Astronomy, University of New Hampshire,
9 Library Way, Durham New Hampshire 03824, USA*


²*Department of Physics, University of California, Berkeley, Berkeley, California 94720, USA*

³*Department of Physics and Astronomy, Washington State University, Pullman, Washington 99164, USA*

⁴*Cornell Center for Astrophysics and Planetary Science, Cornell University, Ithaca, New York 14853, USA*

⁵*Max Planck Institute for Gravitational Physics (Albert Einstein Institute),
Am Mühlenberg 1, D-14476 Potsdam, Germany*

⁶*Theoretical Astrophysics, Walter Burke Institute for Theoretical Physics,
California Institute of Technology, Pasadena, California 91125, USA*

 (Received 6 May 2024; accepted 9 July 2024; published 7 August 2024)

The conformal flatness approximation to the Einstein equations has been successfully used in many astrophysical applications such as initial data constructions and dynamical simulations. Although it has been shown that full general relativistic strongly differentially rotating equilibrium models deviate by at most a few percentage from their conformally flat counterparts, whether those conformally flat solutions remain stable has not been fully addressed. To further understand the limitations of the conformal flatness approximation, in this work, we construct spatially conformally flat hot hypermassive neutron stars with postmergerlike rotation laws, and perform conformally flat evolutions and analysis over dynamical timescales. We find that enforcing conformally flat spacetime could change the equilibrium of quasitoroidal models with high angular momentum for $J \gtrsim 9 GM_{\odot}^2/c$ compared to fully general relativistic cases. In contrast, all the quasispherical models considered in this work remain stable even with high angular momentum $J = 9 GM_{\odot}^2/c$. Our investigation suggests that the quasispherical models are suitable initial data for long-lived hypermassive neutron star modeling in conformally flat spacetime.

DOI: [10.1103/PhysRevD.110.043015](https://doi.org/10.1103/PhysRevD.110.043015)

I. INTRODUCTION

The detection of a binary neutron star merger on August 17, 2017, has laid a milestone in multimessenger astronomy. This event was observed by the coincident detections of gravitational waves GW170817 [1], the short gamma-ray burst GRB170817A [2], and in other spectral bands [3]. Even though this groundbreaking multimessenger detection has confirmed our basic understanding of neutron star mergers [4,5], details of the postmerger evolution are poorly understood. A hypermassive neutron star, which is expected to be hot and supported by strong differential rotation, is one of the possible outcomes of binary neutron star merger. Studying a hypermassive neutron star helps us to further understand the nature of the central engine of the relativistic jets [2,6] and kilonova transients [7–10].

Detailed investigations of the postmerger phase over dynamical and secular timescales are extremely challenging yet significant. Not only does one need to solve Einstein

field equations and general-relativistic magnetohydrodynamics self-consistently [5], neutrino microphysics is also required [11]. Moreover, to better understand the postmerger observational signatures, seconds-long simulations are required. Hence, any simplification of the simulations is highly desirable.

The spatially conformally flat spacetime approximation [12–14] has shown to be useful for modeling neutron star mergers. Binary neutron star merger simulations based on the conformally flat approximation have been successfully carried out (e.g., [15–20]; see also the applications in the context of core-collapse supernovae [21–23] and isolated neutron stars [24–34]). In addition, it has been shown in fully general relativistic simulations that long-lived neutron star merger remnants are qualitatively axisymmetric, and the corresponding spacetime is nearly conformally flat [35,36]. Mapping such postmerger profiles by assuming conformally flat conditions onto other evolution codes that impose different symmetries or with different input physics has been done recently [35,36]. Specifically, the multigrid based conformally flat spacetime solver of Gmunu [37,38] has been demonstrated to be very effective for the studies of

*Contact author: patrick.cheong@berkeley.edu

long-lived postmerger neutron star merger remnants over secular timescales [36].

Understanding the limitation of the conformally flat spacetime approximation in the context of hypermassive neutron stars is critical. Despite the success in neutron star modeling (e.g., [15–20]), the conformally flat condition is ultimately an approximation. This approximation is no longer valid in the case of a Kerr black hole [39,40], and it may also fail with systems that have extreme rotation or high angular momentum. Studies have shown that the local and integrated quantities are at most a few percentage difference between fully general relativistic and conformally flat differentially rotating equilibrium models [41–44]. However, whether the full and conformally flat solutions share the same properties of dynamical and secular stabilities is not clearly addressed. Recently, the conformally flat approximated dynamical evolutions of quasitoroidal models with the J -constant rotation law [45] with polytropic equation of state has been carried out [46]. Nevertheless, the rotation law considered in [46] is very different from that of postmerger remnants. It is still unclear whether postmergerlike hypermassive neutron stars can be accurately modeled under the conformal flatness approximation.

In this work, we investigate the limitations of the conformally flat approximation in high angular momentum postmergerlike hypermassive neutron star modeling. In particular, we construct spatially conformally flat postmergerlike hot hypermassive neutron stars, and perform evolutions and analysis over dynamical timescales. We find that the stellar profiles of conformally flat quasitoroidal models with high angular momentum for $J \gtrsim 9 GM_{\odot}^2/c$ can be distorted noticeably over dynamical timescales even in fully general relativistic evolutions. However, the fully general relativistic variant of such stars remains stable in fully general relativistic evolutions within the time we simulated. This implies that a conformally flat approximation either makes such a high angular momentum star not an equilibrium or makes it an unstable equilibrium. On the other hand, all the quasispherical models considered in this work remain stable even with high angular momentum $J = 9 GM_{\odot}^2/c$. Our study suggests that the quasispherical models are a better choice to be used as hypermassive neutron star modeling because of their rotation properties and stabilities.

The paper is organized as follows. In Sec. II we outline the methods we used in this work. The results are presented in Sec. III. This paper ends with a discussion in Sec. IV. Unless explicitly stated, we use the units in which the speed of light c , gravitational constant G , and solar mass M_{\odot} are all equal to 1 ($c = G = M_{\odot} = 1$).

II. METHODS

A. Initial conditions

Conformally flat, axisymmetric, differentially rotating hot neutron stars in quasiequilibrium are constructed using the

RotNS code [47], and serve as our initial data. RotNS [47] was used to construct equilibrium sequences of rotating polytropes in general relativity. The code has been recently updated to support tabulated equations of state and the four-parameter rotation law of Uryū *et al.* [48]. For the implementation details, we refer readers to [49]. Below, we will only highlight the key setup of the initial data construction.

Although RotNS [47] is a fully general relativistic code, the spatially conformally flat conditions can easily be enforced by imposing an additional condition of the metric potentials, as shown in [41–44]. Here we adopt the same modification in RotNS to construct conformally flat initial data. Unless explicitly stated, all the initial data are constructed in conformally flat spacetime. To construct mergerlike hypermassive neutron star profiles, we adopt the four-parameter rotation law of Uryū *et al.* [48]. In particular, we implement the following rotation law:

$$\Omega(j; \Omega_c) = \Omega_c \frac{1 + [j/(B^2 \Omega_c)]^p}{1 + [j/(A^2 \Omega_c)]^{q+p}}, \quad (1)$$

where j is the specific angular momentum; Ω_c is the central angular velocity of the star; while A , B , q , and p are parameters. In this work, we choose $p = 1$ and $q = 3$. Note that this rotation profile is nonmonotonic, with the maximum angular velocity Ω_{\max} between the center and surface. The characteristic of the models can be controlled by specifying parameters A and B . Alternatively, parameters A and B can be obtained by fixing angular velocity ratios Ω_{\max}/Ω_c and $\Omega_{\text{eq}}/\Omega_c$ [43,44,48], where Ω_{eq} is the equatorial angular velocity of the star. Different choices of the angular velocity ratios can result in either quasitoroidal or quasispherical models.

In this work, we consider two sets of the ratios $\{\Omega_{\max}/\Omega_c, \Omega_{\text{eq}}/\Omega_c\}$, namely, (i) $\{2, 0.5\}$ which results in quasitoroidal models, and (ii) $\{1.6, 1\}$ which results in quasispherical models (see Fig. 1 for examples of the rest

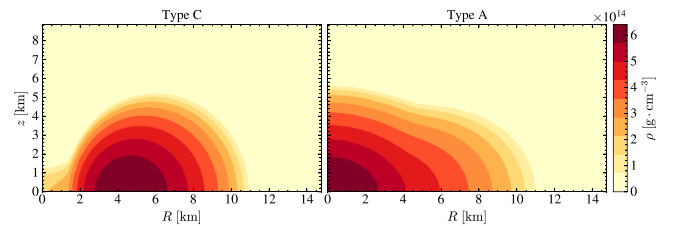


FIG. 1. Two-dimensional rest mass density profiles ρ in the units of $[\text{g cm}^{-3}]$ of the rotating neutron star models. Left panel: quasitoroidal (type C) model with $\{\Omega_{\max}/\Omega_c = 2, \Omega_{\text{eq}}/\Omega_c = 0.5\}$. This star has the angular momentum $J = 11 GM_{\odot}^2/c$ with the maximum energy density $\epsilon_{\max} = 7.073 \times 10^{14} \text{ g cm}^{-3}$. Right panel: quasispherical (type A) model with $\{\Omega_{\max}/\Omega_c = 1.6, \Omega_{\text{eq}}/\Omega_c = 1\}$. This star has the angular momentum $J = 9 GM_{\odot}^2/c$ with the maximum energy density $\epsilon_{\max} = 9.411 \times 10^{14} \text{ g cm}^{-3}$.

mass density profiles of both types of stars). They can be classified as type C and type A solutions according to [50]. Note that the latter set of the ratios is chosen to match the results of the numerical relativity simulations of binary neutron star mergers (e.g., [51,52]; see [43,44]). Therefore, the quasispherical type models are by construction more “postmergerlike” compared to quasitoroidal models.

All the equilibrium models in this work are constructed with equation of state DD2 [53] with a constant entropy per baryon $s = 1 k_B/\text{baryon}$ and in neutrinoless β equilibrium. The temperature is roughly 30 MeV at the center of the star. Note that, such a choice of entropy profile and the resulting temperature profile do not match the numerical relativity simulations, where the temperature at the center is expected to be lower than the surface. Nevertheless, we consider only the constant entropy profile for simplicity. The investigations of different choice of entropy profiles will be left as future work. The resolution of the compacted radius and angular grid (see their definitions in [47]) in RotNS is 600×600 .

B. Simulation setup

We employ the general relativistic magnetohydrodynamics code Gmnu [37,38,54–56] to evolve the neutron star models in dynamical conformally flat spacetime. All the simulations here are axisymmetric (i.e., two-dimensional) in cylindrical coordinates (R, z) , where the computational domain covers $0 \leq R \leq 120$ and $0 \leq z \leq 120$, with the

resolution $n_R \times n_z = 128 \times 128$ and allowing six adaptive mesh refinement levels. The finest grid size at the center of the star is $\Delta R = \Delta z \approx 43.27$ m. The refinement is fixed after the initialization since we do not expect the stars to expand significantly.

Our simulations adopt Harten, Lax and van Leer approximated Riemann solver [57], third-order reconstruction method PPM [58], and third-order accurate SSPRK3 time integrator [59]. Finite temperature equation of state DD2 [53] is used for the evolutions. Although neutrinos are not included, the electron fraction Y_e is evolved in these simulations.

The rest-mass density of the atmosphere ρ_{atmo} is set to be $10^{-10} \rho_{\text{max}}(t=0)$. For anywhere that the matter has rest-mass density lower than ρ_{atmo} , we reset the rest-mass density of those regions to be $0.2\rho_{\text{atmo}}$, and zero the velocities (i.e., $v^i = 0$). As a result, the angular velocity $\Omega \equiv \alpha v^\phi - \beta^\phi$ has a sudden drop at the neutron star surface at $t = 0$ (see, e.g., Fig. 3). These areas will be filled with low density gas that rotates with similar angular velocity as soon as the simulation started, and do not affect the dynamics of the neutron star because of the ultralow rest-mass density.

To initialize the simulations, we map the conservative variables of the stars into Gmnu, and solve the metric again with the multigrid metric solver [37,38]. This approach can also be applied on fully general relativistic profiles, which was used in [35,36].

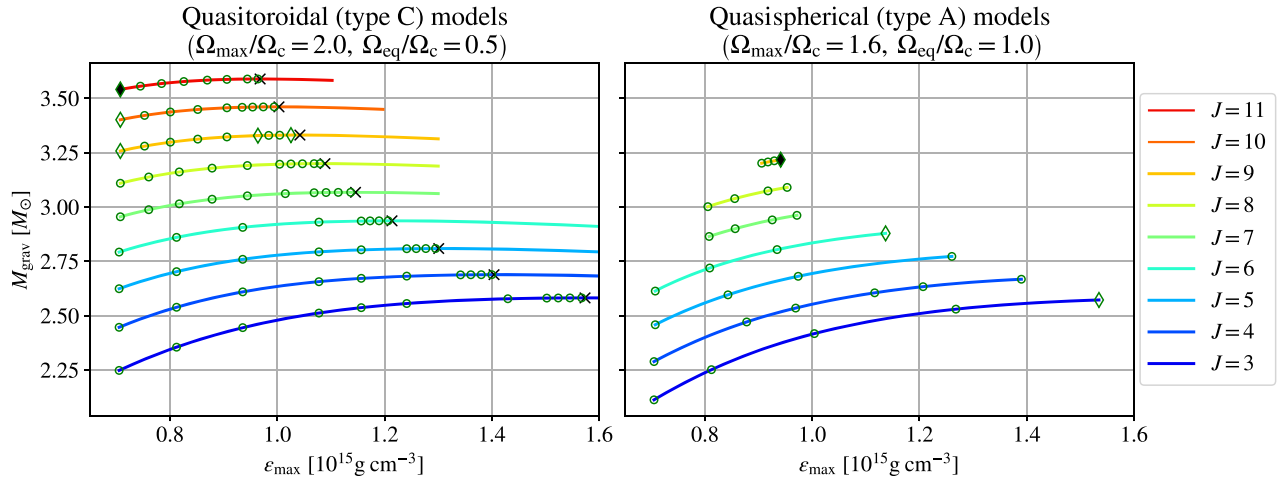


FIG. 2. Gravitational mass M_{grav} versus maximum energy density ϵ_{max} for various constant angular momentum sequences. Circles and diamonds mark the dynamically evolved models without introducing perturbations. The diamonds refer to the models presented in detail in Figs. 3, 4, and 7. The black diamonds are the two cases presented in Fig. 1. None of the simulations presented here collapse as black holes. Left panel: quasitoroidal (type C) model with $\{\Omega_{\text{max}}/\Omega_{\text{c}} = 2, \Omega_{\text{eq}}/\Omega_{\text{c}} = 0.5\}$. The angular momentum J ranges from 3 to 11 GM_{\odot}^2/c . The J -constant turning points are marked with black crosses. We find that models with high angular momentum (i.e., $J \gtrsim 9$) fail to preserve their stellar profiles; see Figs. 3 and 4 and the discussions in Sec. III B. Right panel: quasispherical (type A) model with $\{\Omega_{\text{max}}/\Omega_{\text{c}} = 1.6, \Omega_{\text{eq}}/\Omega_{\text{c}} = 1\}$. The angular momentum J ranges from 3 to 9 GM_{\odot}^2/c . In this type of model, we do not observe J -constant turning points. The RotNS code fails to converge when the maximum energy density goes beyond the plotted values, which agrees with [44]. All the dynamically evolved models remain stable up to 20 ms evolutions.

III. RESULTS

A. Sequences of equilibrium models

Figure 2 shows the gravitational mass M_{grav} versus maximum energy density ϵ_{max} of constant angular momentum sequences constructed in this work. Note again that the spatial conformally flat condition is enforced in all the sequences reported here. Circles and diamonds mark the

dynamically evolved models without introducing perturbations. The diamonds refer to the models presented in detail in Figs. 3, 4, and 7. None of the simulations presented here collapses as black holes. However, we note that these noncollapsing models are not necessarily stable; see further discussions in Secs. III B and III C below.

The left panel of Fig. 2 shows quasitoroidal (type C) models with $\{\Omega_{\text{max}}/\Omega_{\text{c}} = 2, \Omega_{\text{eq}}/\Omega_{\text{c}} = 0.5\}$, where the

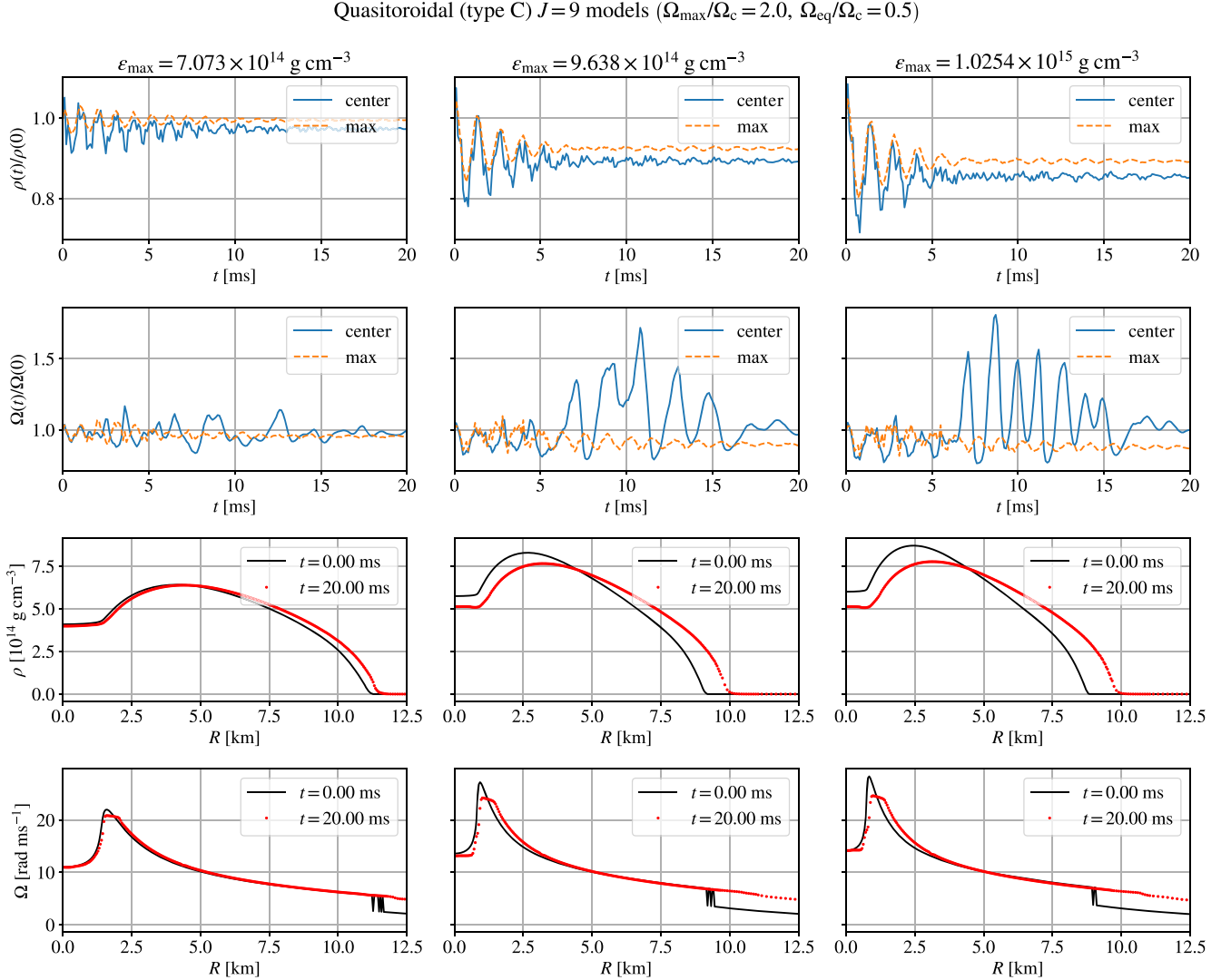


FIG. 3. Comparison of the dynamical evolutions of the quasitoroidal (type C) models with angular momentum $J = 9$ with different maximum energy densities ϵ_{max} . Three cases are shown in this plot, namely, $\epsilon_{\text{max}} = 7.073 \times 10^{14} \text{ g cm}^{-3}$ (left column), $\epsilon_{\text{max}} = 9.638 \times 10^{14} \text{ g cm}^{-3}$ (middle column), and $\epsilon_{\text{max}} = 1.0254 \times 10^{15} \text{ g cm}^{-3}$ (right column), respectively. The first and second rows show the relative variation of the rest mass densities and angular velocities in time (blue solid lines are for central values while the orange dashed lines are for maximum values). In all cases, the rest mass densities oscillate, and gradually settle to a slightly lower value. The central angular velocity Ω_{c} oscillates strongly at around 10 ms, but relaxes back to initial values later. For the high maximum energy density ϵ_{max} case, the final central rest mass density $\rho_{\text{c}}(t = 20 \text{ ms})$ is about 18% smaller than the initial value. The third and fourth rows compare the initial (black solid lines) and final ($t = 20 \text{ ms}$, red dots) profiles of the rest mass density ρ and the angular velocity Ω along R axis (i.e., $z = 0$). The higher the maximum energy density ϵ_{max} is, the lower of the final maximum rest mass density ρ_{max} , and the stronger the distortion of the rest mass density ρ and the angular velocity Ω profiles. Despite the significant distortions of the rest mass density profiles $\rho(R, z = 0)$, the angular velocity profiles $\Omega(R, z = 0)$ in all the cases considered here are qualitatively preserved.

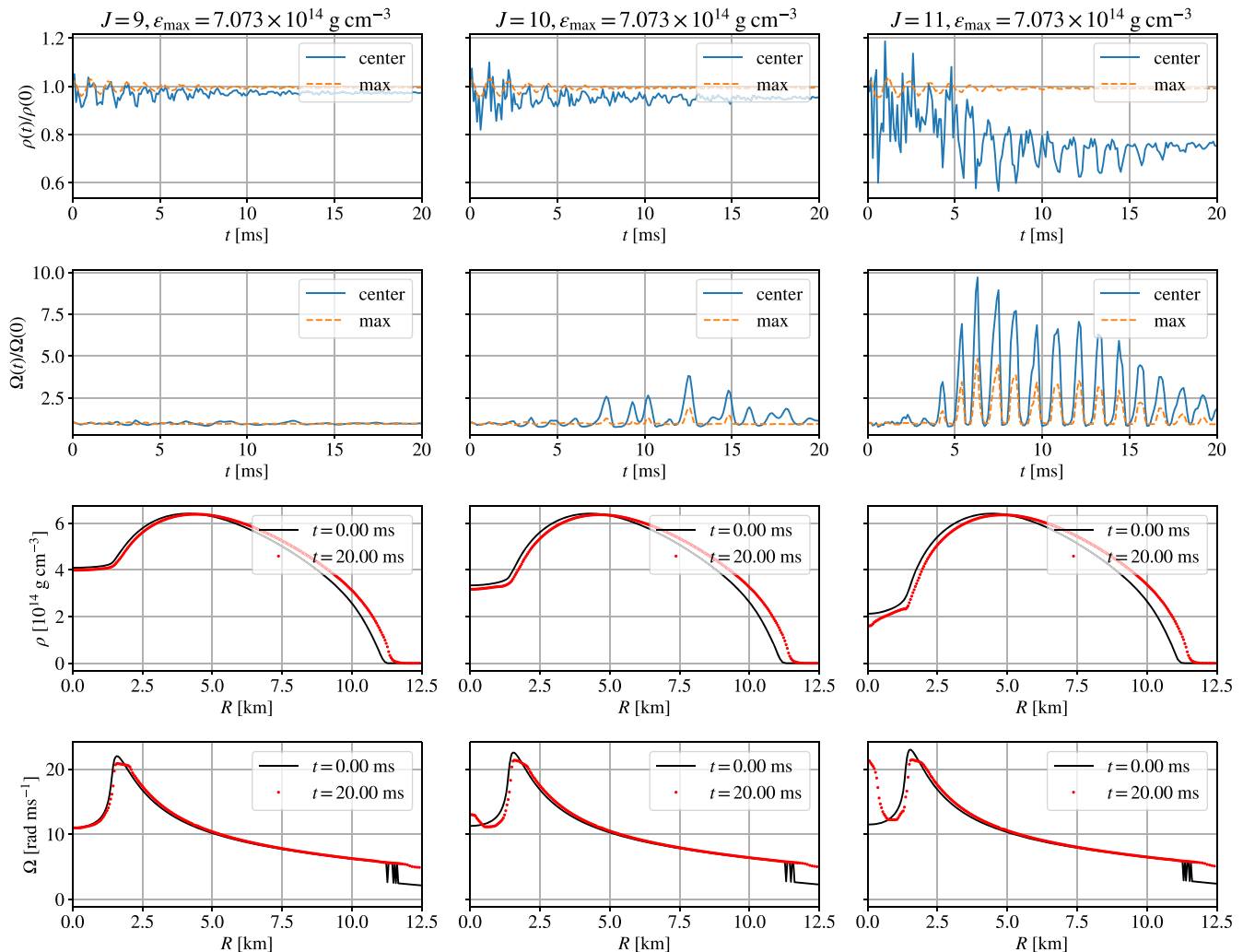
Quasitoroidal (type C) models ($\Omega_{\max}/\Omega_c = 2.0$, $\Omega_{\text{eq}}/\Omega_c = 0.5$)


FIG. 4. Comparison of the dynamical evolutions of the quasitoroidal (type C) models with maximum energy density $\epsilon_{\max} = 7.073 \times 10^{14} \text{ g cm}^{-3}$ with high angular momentum $J \geq 9$. Three cases are shown in this plot, namely, $J = 9$ (left column), $J = 10$ (middle column), and $J = 11$ (right column), respectively. The first and second rows show the relative variation of the rest mass densities and angular velocities in time (blue solid lines are for central values while the orange dashed lines are for maximum values). The third and fourth rows compare the initial ($t = 0.00$ ms, black solid lines) and final ($t = 20.00$ ms, red dots) profiles of the rest mass density ρ and the angular velocity Ω along the R axis. The angular velocity profile $\Omega(R, z = 0)$ for $J > 9$ cases changes significantly at the center of the stars, and the rotation law of Uryū *et al.* [48] no longer holds. Moreover, in the highest angular momentum $J = 11$ case, although the change of the maximum rest mass density ρ_{\max} is small, the central rest mass density ρ_c decreases by about 20% compared to the initial value. Both the central and maximum angular velocities oscillate quasiperiodically. The amplitudes of the oscillation are very large; the angular velocities can be a few times higher during the evolutions. Note that all the models presented in this plot are the least massive models at a given angular momentum (i.e., far from the J -turning points); such strong oscillations and deformations of the stars are unexpected.

angular momentum J ranges from 3 to $11 GM_{\odot}^2/c$. The J -constant turning points are observed in all the quasitoroidal sequences, which are marked with black crosses in the plot. According to the turning point criterion [45], the J -constant turning points mark the onset of instability. However, this is not an exact threshold to collapse. The situation becomes more complicated for differentially rotating cases. The stability and maximum mass of differentially rotating stars with J -constant rotation law [45] has been studied

[46,60,61]. More recently, Muhammed *et al.* [49] show that the turning point criterion seems to also hold in the cases of Uryū *et al.* [48] rotation law. In this work, we only dynamically evolve the models that have smaller maximum energy density ϵ_{\max} than the J -constant turning points.

The right panel of Fig. 2 on the other hand shows the quasispherical (type A) model with $\{\Omega_{\max}/\Omega_c = 1.6, \Omega_{\text{eq}}/\Omega_c = 1\}$, where the angular momentum J ranges from 3 to $9 GM_{\odot}^2/c$. Unlike the quasitoroidal cases, we do not

observe J -constant turning points in these sequences. As the maximum energy density ϵ_{\max} goes beyond the plotted values, the RotNS code fails to converge. This behavior agrees with the discussion in the Section III B in [44]. The origin of this issue is still unknown, which is beyond the scope of this work and will be investigated in a future study.

B. Evolutions of quasitoroidal profiles

In this subsection, we present some evolutions of the quasitoroidal (type C) models with different angular momentum J and maximum energy density ϵ_{\max} . All the models considered here have lower maximum energy density ϵ_{\max} than the J -constant turning points. We do not introduce any perturbations into the evolutions. Since all the low angular momentum cases are found to be stable

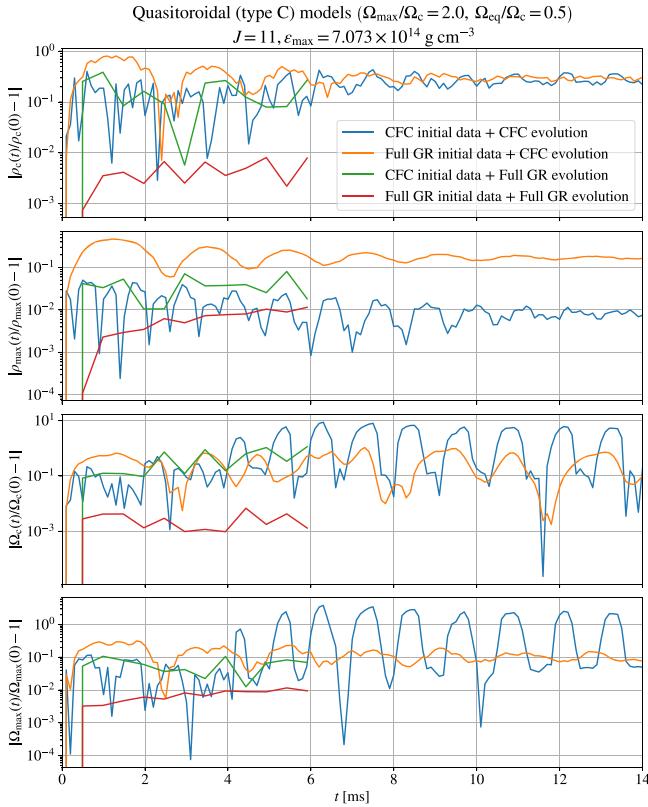


FIG. 5. The relative variation of the central and maximum rest mass densities and angular velocities of the same models with or without conformally flat approximation. The quasitoroidal (type C) models with maximum energy density $\epsilon_{\max} = 7.073 \times 10^{14} \text{ g cm}^{-3}$ with angular momentum $J = 11$ are used in these simulations. All the evolutions have significant deviations except cases where both the initial profile and evolution are fully general relativistic (red lines). Although the conformally flat equilibrium solutions have only a few percentage deviations from their fully general relativistic counterpart [41–44], the dynamical stabilities of high angular momentum equilibrium models could be changed under conformally flat approximation.

and trivial, in this section we discuss only the high angular momentum cases (i.e., $J \geq 9$).

Figure 3 compares the dynamical evolutions of the quasitoroidal (type C) models with angular momentum $J = 9$ with different maximum energy densities ϵ_{\max} . In all cases, the maximum rest mass densities ρ_{\max} oscillate, and gradually relax to a slightly lower value. For the high maximum energy density $\epsilon_{\max} = 1.0245 \times 10^{15} \text{ g cm}^{-3}$ case, the final central rest mass density $\rho_c(t = 20 \text{ ms})$ is about 18% smaller than the initial value, which is not ignorable and indicates that the star migrates into another configuration. The rest mass density ρ and the angular velocity Ω along the R axis (i.e., $z = 0$) at the end of the simulation ($t = 20 \text{ ms}$) are significantly distorted except in the low maximum energy density case. The distortions are stronger in the higher maximum energy density ϵ_{\max} cases. Although none of these neutron stars collapse to black holes, the medium and high energy density cases were not stable against the evolution up to 20 ms.

Figure 4 compares the dynamical evolutions of also the quasitoroidal models with maximum energy density $\epsilon_{\max} = 7.073 \times 10^{14} \text{ g cm}^{-3}$ with high angular momentum $J \geq 9$. The evolutions of the rest mass densities behave similarly, i.e., they oscillate, and gradually relax to a lower value. The higher the angular momentum J is, the stronger the distortion of the rest mass density ρ and the angular

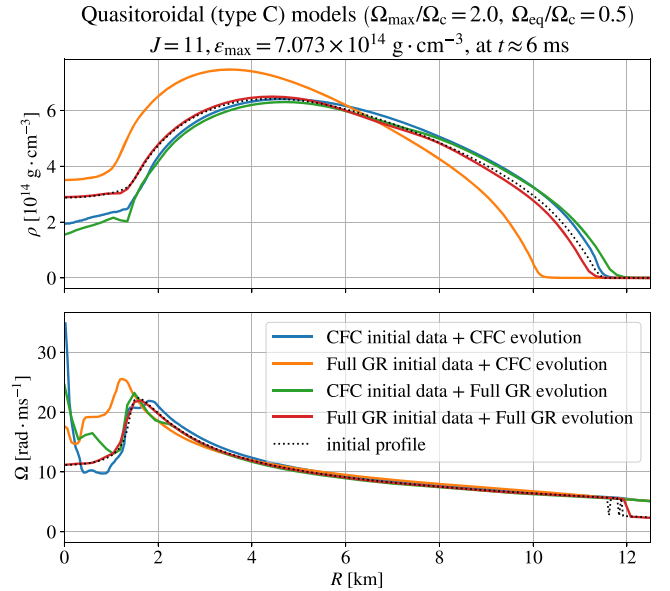


FIG. 6. Comparison of the rest mass density and angular velocity profiles at the beginning ($t = 0 \text{ ms}$, black dotted lines) and at $t \approx 6 \text{ ms}$ (solid lines) of the same models with or without conformally flat approximation. The quasitoroidal (type C) models with maximum energy density $\epsilon_{\max} = 7.073 \times 10^{14} \text{ g cm}^{-3}$ with angular momentum $J = 11$ are used in these simulations. The profiles are well preserved only in the case where both the initial profile and evolution are fully general relativistic (red lines).

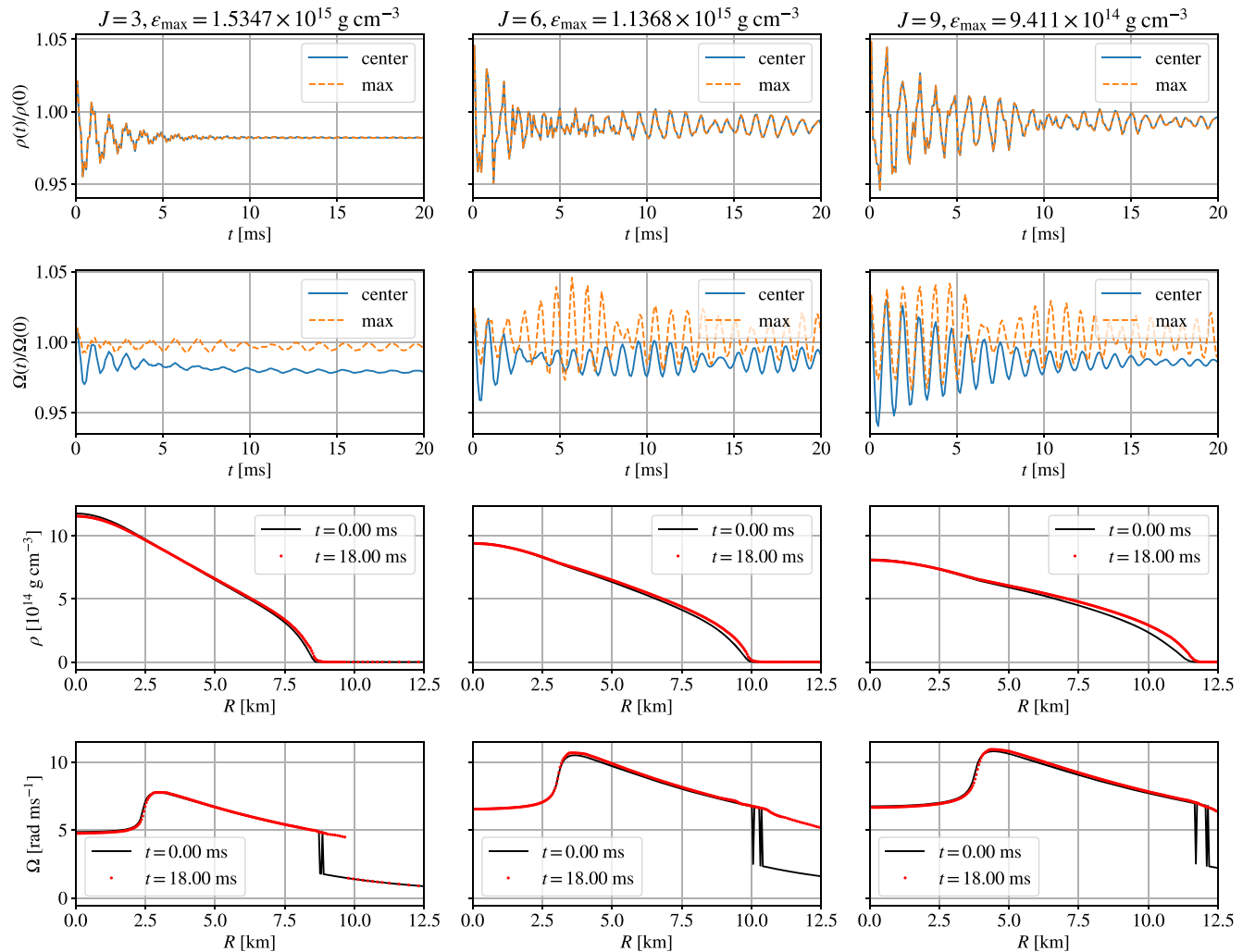
Quasispherical (type A) models ($\Omega_{\max}/\Omega_c = 1.6$, $\Omega_{\text{eq}}/\Omega_c = 1.0$)


FIG. 7. Comparison of the dynamical evolutions of the quasispherical (type A) models with different maximum energy densities ϵ_{\max} and angular momentum J . In this plot, we show the most massive models with three given angular momentum, i.e., $J = 3$ (left column), $J = 6$ (middle column), and $J = 9$ (right column). The first and second rows show the relative variation of the rest mass densities and angular velocities in time (blue solid lines are for central values while the orange dashed lines are for maximum values). The evolutions of the maximum and central rest mass densities ρ are identical in the quasispherical models. All the relative variations shown here are within 5%. The third and fourth rows compare the rest mass density ρ and the angular velocity Ω profiles along the R axis at the beginning ($t = 0$ ms, black solid lines) and a later time $t = 18$ ms (red dots). As shown at the first two rows, the $J = 6$ and $J = 9$ models are not yet relaxed to stationary states by the end of the simulations ($t = 20$ ms); the oscillation is still noticeable in the scale we are plotting. Such oscillations result in small quasiperiodic distortions of the stellar profiles (e.g., angular velocity Ω). Therefore, instead of plotting the profiles at the end of the simulations, we pick the slightly earlier time (i.e., at $t = 18$ ms) for better visualizations. Unlike the cases in quasitoroidal (see Figs. 4 and 3), the profiles are preserved better in this case, and the decrease of the maximum rest mass density ρ is about 2% even for the most massive case with the highest angular momentum $J = 9$. These results suggest that these quasispherical (type A) models are dynamically stable in conformally flat simulations within 20 ms.

velocity Ω profiles. Although the maximum energy density of all the models considered here are noticeably lower than the J -constant turning points, we found that the angular velocity profiles $\Omega(R, z)$ are not preserved in some high angular momentum cases. For instance, in the highest angular momentum $J = 11$ case, the central rest mass density ρ_c decreases significantly by about 20% compared

to the initial value. Also, the angular velocity profile $\Omega(R, z = 0)$ changes significantly at the center of the stars; the rotation law of Uryū *et al.* [48] is violated. Both the central and maximum angular velocities oscillate quasiperiodically with large amplitudes; the angular velocities can sometime be a few times higher than the initial values during the evolutions. Note again that all the models

presented in this plot are the least massive models at a given angular momentum (i.e., far from the J -turning points); such strong oscillations and deformations of the stars are unexpected.

1. Comparison to fully general relativistic cases

To better understand the origin of the nonstable behavior, we further compare different combinations of conformally flat and fully general relativistic initial profiles and evolutions of selected quasitoroidal (type C) models. In this section, we focus on the quasitoroidal (type C) model with maximum energy density $\epsilon_{\max} = 7.073 \times 10^{14} \text{ g cm}^{-3}$ with angular momentum $J = 11$. The Spectral Einstein Code (SpEC) [62] is used for the fully general relativistic evolutions. The details of the numerical setup in SpEC can be found at [49,63].

In this subsection, we consider four cases, namely, (i) conformally flat initial data with conformally flat evolution; (ii) general relativistic initial data with conformally flat evolution; (iii) conformally flat initial data with fully general relativistic evolution; and (iv) general relativistic initial data with fully general relativistic evolution. One may argue that it is not necessary to consider case (ii) since it is more or less similar to case (i). After all, nonspherically symmetric full general relativistic initial data are in general not conformally flat, and there is no self-consistent way to map such initial data into a conformally flat evolution code. To evolve such a star, we solve the conformally flat metric equations with the conserved variables of the fully general relativistic star, as discussed in Sec. II B. This is effectively enforcing the initial data to be conformally flat at the beginning. However, this does not guarantee that the profile will still be an equilibrium. In this work, we nevertheless include this case to discuss the validity of mapping a fully general relativistic profile into a conformally flat evolution code as in [36].

Comparisons of the rest mass densities and angular velocities of the same models with or without a conformally flat approximation are shown in Figs. 5 and 6. In particular, Fig. 5 shows the absolute values of the relative variation of the central and maximum rest mass densities and angular velocities while Fig. 6 compares the profiles at $t \approx 6 \text{ ms}$. Interestingly, the conformally flat initial profile is always unstable even with fully general relativistic evolution. The star remains stable only when the profile and evolution are fully general relativistic [case (iv), red lines]. This implies that the conformally flat approximation either makes such a high angular momentum star not an equilibrium or makes it an unstable equilibrium.

C. Evolutions of quasispherical profiles

In this subsection, we present some evolutions of the quasispherical (type A) models with different angular momentum J and maximum energy density ϵ_{\max} . As

mentioned, we do not observe any J -constant turning points when we construct the fixed angular momentum sequences. Therefore, we simulate models at both ends, i.e., from low to high maximum energy density ϵ_{\max} .

Figure 7 compares the dynamical evolutions of the quasispherical (type A) models with the most massive models at three given angular momentums, $J = 3$, $J = 6$, and $J = 9$. Although they are the most extreme type A models we have constructed, all of them are dynamically stable in conformally flat simulations. Indeed, all the simulations we have done (the green circles in the right panel of Fig. 2) of this type of model remain stable.

IV. DISCUSSION

The goal of this work is to investigate how well the differentially rotating quasiequilibrium models with high angular momentum remain stable in spatially conformally flat simulations. To this end, we have constructed both quasitoroidal and quasispherical types of spatially conformally flat mergerlike hot hypermassive neutron stars. In particular, the ‘‘postmergerlike’’ rotation law of Uryū *et al.* [48] is introduced, and assumes constant entropy per baryon $s = 1 k_B/\text{baryon}$ and in neutrinoless β equilibrium. We further assess their stability by performing dynamical simulations in conformally flat spacetime using Gmunu.

We show that a conformally flat approximation could alter the dynamical stability of the quasitoroidal models despite only a few percentage difference with their fully general-relativistic variation [41–44]. Our simulations show that not all conformally flat quasitoroidal models remain dynamically stable even for cases where the maximum energy density ϵ_{\max} is considerably smaller than the J -constant turning points. In high angular momentum (i.e., $J \gtrsim 9$) conformally flat cases, both the rest mass density and angular velocity can be distorted significantly even with fully general relativistic evolutions. However, this is not the case when both the initial profile and evolutions are fully general relativistic. This implies that a conformally flat approximation either makes such a high angular momentum star not an equilibrium or makes it an unstable equilibrium. Mapping these stellar profiles from fully general relativistic simulations to other codes by assuming conformally flat conditions (e.g., [35,36]) could result in a very different lifetime of the star, therefore affecting the modeling of the matter outflow. The origin of such behavior can be better understood by studying its hydrodynamical instability (e.g., [64]), which is left as future work.

On the other hand, unlike the quasitoroidal models, we show that all the quasispherical models considered in this work remain stable. The quasispherical models are not only by construction more postmergerlike compared to the quasitoroidal models; they are dynamically stable even for the most extreme cases we considered. These properties make them ideal choices for long-lived hypermassive

neutron star modeling. Generating different sequences with different parameters (e.g., mass, angular momentum, equation of state) enables us to systemically study how these parameters affect the outcomes of the postmerger. In the future, we will attempt to deliver postmerger modeling with such quasispherical models together with magnetic fields and neutrino transport.

ACKNOWLEDGMENTS

P. C. K. C. gratefully acknowledges support from NSF Grant No. PHY-2020275 [Network for Neutrinos, Nuclear Astrophysics, and Symmetries (N3AS)]. F. F. gratefully acknowledges support from the Department of Energy, Office of Science, Office of Nuclear Physics, under Contract No. DE-AC02-05CH11231 and from the NSF through Grant No. AST-2107932. M. D. gratefully acknowledges support from the NSF through Grant No. PHY-2110287. M. D. and F. F. gratefully acknowledge support from NASA through Grant No. 80NSSC22K0719. P. C. K. C. is N3AS Postdoctoral fellow. The simulations in this work have been performed on the third UNH supercomputer Marvin, also known as Plasma, which is supported by the NSF/MRI program under Grant No. AGS-1919310. The data of the simulations were postprocessed and visualized with YT [65], NumPy [66], PANDAS [67,68], SciPy [69], and Matplotlib [70,71].

APPENDIX: CONVERGENCE TESTS

Here we present the convergence tests. The simulations have the same setup as in the paper, except that we introduce initial ingoing velocity perturbation, as shown in Fig. 8. As shown in the plot, the oscillation amplitudes are mostly the same at the very beginning, and gradually decrease as time goes on. At low resolution, the simulations are very diffusive, and relax to the stationary state sooner.

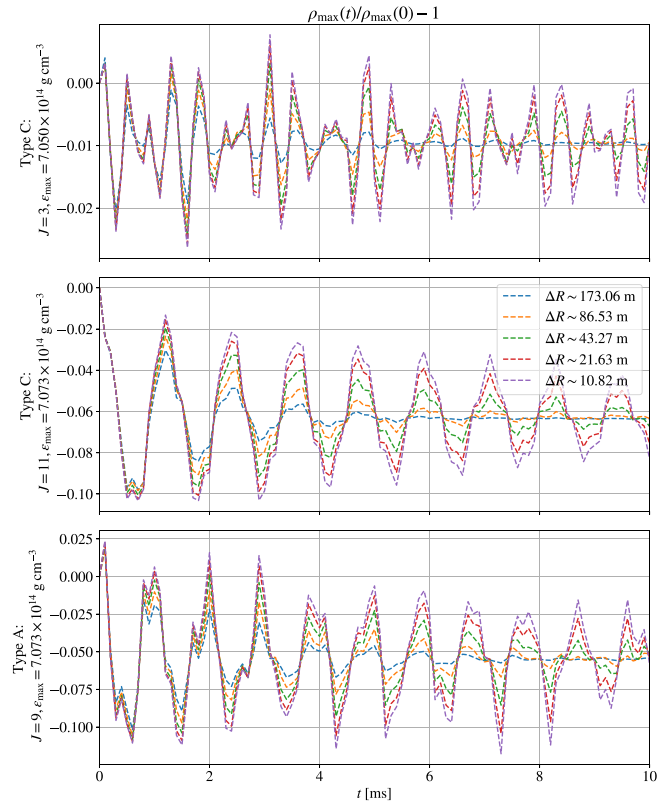


FIG. 8. The relative variation of the maximum rest mass density ρ_{\max} with different resolution in different models. Upper panel: quasitoroidal (type C) model with $J = 3$, $\epsilon_{\max} = 7.050 \times 10^{14} \text{ g cm}^{-3}$. Middle panel: quasitoroidal (type C) model with $J = 11$, $\epsilon_{\max} = 7.073 \times 10^{14} \text{ g cm}^{-3}$. Lower panel: quasispherical (type A) model with $J = 9$, $\epsilon_{\max} = 7.073 \times 10^{14} \text{ g cm}^{-3}$. Initial ingoing velocity perturbation is introduced in these simulations. As shown in the plot, the oscillation amplitudes are mostly the same at the very beginning, and gradually decrease as time goes on. At low resolution, the simulations are very diffusive, which relaxes the oscillation sooner.

- [1] B. P. Abbott, R. Abbott, T. D. Abbott, F. Acernese, K. Ackley, C. Adams, and T. Adams, GW170817: Observation of gravitational waves from a binary neutron star inspiral, *Phys. Rev. Lett.* **119**, 161101 (2017).
- [2] B. P. Abbott, R. Abbott, T. D. Abbott, F. Acernese, K. Ackley, C. Adams, and T. Adams, Gravitational waves and gamma-rays from a binary neutron star merger: GW170817 and GRB 170817A, *Astrophys. J. Lett.* **848**, L13 (2017).
- [3] B. P. Abbott, R. Abbott, T. D. Abbott, F. Acernese, K. Ackley, C. Adams, and T. Adams, Multi-messenger observations of a binary neutron star merger, *Astrophys. J. Lett.* **848**, L12 (2017).
- [4] B. D. Metzger, Welcome to the multi-messenger era! Lessons from a neutron star merger and the landscape ahead, [arXiv:1710.05931](https://arxiv.org/abs/1710.05931).
- [5] L. Rezzolla, P. Pizzochero, D. I. Jones, N. Rea, and I. Vidaña, *The Physics and Astrophysics of Neutron Stars*, Astrophysics and Space Science Library (Springer, Cham, 2018), Vol. 457, pp. XIX, 811.
- [6] E. Berger, Short-duration gamma-ray bursts, *Annu. Rev. Astron. Astrophys.* **52**, 43 (2014).
- [7] L.-X. Li and B. Paczyński, Transient events from neutron star mergers, *Astrophys. J. Lett.* **507**, L59 (1998).
- [8] B. D. Metzger, G. Martínez-Pinedo, S. Darbha, E. Quataert, A. Arcones, D. Kasen, R. Thomas, P. Nugent, I. V. Panov,

- and N. T. Zinner, Electromagnetic counterparts of compact object mergers powered by the radioactive decay of r-process nuclei, *Mon. Not. R. Astron. Soc.* **406**, 2650 (2010).
- [9] M. Tanaka, Kilonova/macronova emission from compact binary mergers, *Adv. Astron.* **2016**, 634197 (2016).
- [10] B. D. Metzger, Kilonovae, *Living Rev. Relativity* **23**, 1 (2019).
- [11] F. Foucart, Neutrino transport in general relativistic neutron star merger simulations, *Living Rev. Comput. Astrophys.* **9**, 1 (2023).
- [12] J. R. Wilson and G. J. Mathews, *Relativistic Numerical Hydrodynamics*, Cambridge Monographs on Mathematical Physics (Cambridge University Press, Cambridge, England, 2003).
- [13] J. A. Isenberg, Waveless approximation theories of gravity, *Int. J. Mod. Phys. D* **17**, 265 (2008).
- [14] I. Cordero-Carrión, P. Cerdá-Durán, H. Dimmelmeier, J. L. Jaramillo, J. Novak, and E.ourgoulhon, Improved constrained scheme for the Einstein equations: An approach to the uniqueness issue, *Phys. Rev. D* **79**, 024017 (2009).
- [15] R. Oechslin, S. Rosswog, and F.-K. Thielemann, Conformally flat smoothed particle hydrodynamics application to neutron star mergers, *Phys. Rev. D* **65**, 103005 (2002).
- [16] A. Bauswein, H. T. Janka, K. Hebeler, and A. Schwenk, Equation-of-state dependence of the gravitational-wave signal from the ring-down phase of neutron-star mergers, *Phys. Rev. D* **86**, 063001 (2012).
- [17] A. Bauswein, S. Goriely, and H. T. Janka, Systematics of dynamical mass ejection, nucleosynthesis, and radioactively powered electromagnetic signals from neutron-star mergers, *Astrophys. J.* **773**, 78 (2013).
- [18] A. Bauswein, N. Stergioulas, and H. T. Janka, Revealing the high-density equation of state through binary neutron star mergers, *Phys. Rev. D* **90**, 023002 (2014).
- [19] A. Bauswein, S. Blacker, G. Lioutas, T. Soutanis, V. Vijayan, and N. Stergioulas, Systematics of prompt black-hole formation in neutron star mergers, *Phys. Rev. D* **103**, 123004 (2021).
- [20] G. Lioutas, A. Bauswein, T. Soutanis, R. Pakmor, V. Springel, and F. K. Röpkke, General relativistic moving-mesh hydrodynamic simulations with AREPO and applications to neutron star mergers, *Mon. Not. R. Astron. Soc.* **528**, 1906 (2024).
- [21] H. Dimmelmeier, J. A. Font, and E. Müller, Relativistic simulations of rotational core collapse II. Collapse dynamics and gravitational radiation, *Astron. Astrophys.* **393**, 523 (2002).
- [22] M. Saijo, The collapse of differentially rotating supermassive stars: Conformally flat simulations, *Astrophys. J.* **615**, 866 (2004).
- [23] B. Müller, The dynamics of neutrino-driven supernova explosions after shock revival in 2D and 3D, *Mon. Not. R. Astron. Soc.* **453**, 287 (2015).
- [24] H. Dimmelmeier, N. Stergioulas, and J. A. Font, Non-linear axisymmetric pulsations of rotating relativistic stars in the conformal flatness approximation, *Mon. Not. R. Astron. Soc.* **368**, 1609 (2006).
- [25] N. Bucciantini and L. Del Zanna, General relativistic magnetohydrodynamics in axisymmetric dynamical spacetimes: The x-echo code, *Astron. Astrophys.* **528**, A101 (2011).
- [26] H. H.-Y. Ng, P. C.-K. Cheong, L.-M. Lin, and T. G. F. Li, Gravitational-wave asteroseismology with f-modes from neutron star binaries at the merger phase, *Astrophys. J.* **915**, 108 (2021).
- [27] M. Y. Leung, A. K. L. Yip, P. C.-K. Cheong, and T. G. F. Li, Oscillations of highly magnetized non-rotating neutron stars, *Commun. Phys.* **5**, 334 (2022).
- [28] A. K. L. Yip, P. Chi-Kit Cheong, and T. G. F. Li, General-relativistic simulations of the formation of a magnetized hybrid star, [arXiv:2303.16820](https://arxiv.org/abs/2303.16820).
- [29] A. K. L. Yip, P. Chi-Kit Cheong, and T. G. F. Li, Universal relations for fundamental modes of rotating neutron stars with differential rotations, [arXiv:2401.13993](https://arxiv.org/abs/2401.13993).
- [30] N. Bucciantini and L. Del Zanna, General relativistic magnetohydrodynamics in axisymmetric dynamical spacetimes: The X-ECHO code, *Astron. Astrophys.* **528**, A101 (2011).
- [31] A. G. Pili, N. Bucciantini, and L. Del Zanna, Axisymmetric equilibrium models for magnetized neutron stars in general relativity under the conformally flat condition, *Mon. Not. R. Astron. Soc.* **439**, 3541 (2014).
- [32] A. G. Pili, N. Bucciantini, and L. Del Zanna, General relativistic neutron stars with twisted magnetosphere, *Mon. Not. R. Astron. Soc.* **447**, 2821 (2015).
- [33] A. G. Pili, N. Bucciantini, and L. Del Zanna, General relativistic models for rotating magnetized neutron stars in conformally flat space-time, *Mon. Not. R. Astron. Soc.* **470**, 2469 (2017).
- [34] J. Soldateschi, N. Bucciantini, and L. Del Zanna, Axisymmetric equilibrium models for magnetised neutron stars in scalar-tensor theories, *Astron. Astrophys.* **640**, A44 (2020).
- [35] S. Fujibayashi, Y. Sekiguchi, K. Kiuchi, and M. Shibata, Properties of neutrino-driven ejecta from the remnant of a binary neutron star merger: Pure radiation hydrodynamics case, *Astron. Astrophys.* **846**, 114 (2017).
- [36] H. Ho-Yin Ng, J.-L. Jiang, C. Musolino, C. Ecker, S. D. Tootle, and L. Rezzolla, A hybrid approach to long-term binary neutron-star simulations, *Phys. Rev. D* **109**, 064061 (2024).
- [37] P. C.-K. Cheong, L.-M. Lin, and T. G. F. Li, Gmunu: Toward multigrid based Einstein field equations solver for general-relativistic hydrodynamics simulations, *Classical Quantum Gravity* **37**, 145015 (2020).
- [38] P. C.-K. Cheong, A. T.-L. Lam, H. H.-Y. Ng, and T. G. F. Li, Gmunu: Paralleled, grid-adaptive, general-relativistic magnetohydrodynamics in curvilinear geometries in dynamical space-times, *Mon. Not. R. Astron. Soc.* **508**, 2279 (2021).
- [39] A. Garat and R. H. Price, Nonexistence of conformally flat slices of the Kerr spacetime, *Phys. Rev. D* **61**, 124011 (2000).
- [40] J. A. Kroon, Nonexistence of conformally flat slices in Kerr and other stationary spacetimes, *Phys. Rev. Lett.* **92**, 041101 (2004).

- [41] G. B. Cook, S. L. Shapiro, and S. A. Teukolsky, Testing a simplified version of Einstein's equations for numerical relativity, *Phys. Rev. D* **53**, 5533 (1996).
- [42] P. Iosif and N. Stergioulas, On the accuracy of the IWM-CFC approximation in differentially rotating relativistic stars, *Gen. Relativ. Gravit.* **46**, 1800 (2014).
- [43] P. Iosif and N. Stergioulas, Equilibrium sequences of differentially rotating stars with post-merger-like rotational profiles, *Mon. Not. R. Astron. Soc.* **503**, 850 (2021).
- [44] P. Iosif and N. Stergioulas, Models of binary neutron star remnants with tabulated equations of state, *Mon. Not. R. Astron. Soc.* **510**, 2948 (2022).
- [45] J. L. Friedman, J. R. Ipser, and R. D. Sorkin, Turning point method for axisymmetric stability of rotating relativistic stars, *Astrophys. J.* **325**, 722 (1988).
- [46] P. Szewczyk, D. Gondek-Rosińska, and P. Cerdá-Durán, Maximum mass and stability of differentially rotating neutrons stars, *Acta Phys. Pol. B Proc. Suppl.* **16**, 8 (2023).
- [47] G. B. Cook, S. L. Shapiro, and S. A. Teukolsky, Rapidly rotating polytropes in general relativity, *Astrophys. J.* **422**, 227 (1994).
- [48] K. Uryū, S. Yoshida, E. Gourgoulhon, C. Markakis, K. Fujisawa, A. Tsokaros, K. Taniguchi, and Y. Eriguchi, New code for equilibriums and quasiequilibrium initial data of compact objects. IV. Rotating relativistic stars with mixed poloidal and toroidal magnetic fields, *Phys. Rev. D* **100**, 123019 (2019).
- [49] N. Muhammed, M. D. Duez, P. Chawhan, N. Ghadiri, L. T. Buchman, F. Foucart, P. Chi-Kit Cheong, L. E. Kidder, H. P. Pfeiffer, and M. A. Scheel, Stability of hypermassive neutron stars with realistic rotation and entropy profiles, [arXiv:2403.05642](https://arxiv.org/abs/2403.05642).
- [50] M. Ansorg, D. Gondek-Rosińska, and L. Villain, On the solution space of differentially rotating neutron stars in general relativity, *Mon. Not. R. Astron. Soc.* **396**, 2359 (2009).
- [51] M. Hanauske, K. Takami, L. Bovard, L. Rezzolla, J. A. Font, F. Galeazzi, and H. Stöcker, Rotational properties of hypermassive neutron stars from binary mergers, *Phys. Rev. D* **96**, 043004 (2017).
- [52] R. De Pietri, A. Feo, J. A. Font, F. Löffler, M. Pasquali, and N. Stergioulas, Numerical-relativity simulations of long-lived remnants of binary neutron star mergers, *Phys. Rev. D* **101**, 064052 (2020).
- [53] M. Hempel and J. Schaffner-Bielich, A statistical model for a complete supernova equation of state, *Nucl. Phys.* **A837**, 210 (2010).
- [54] P. C.-K. Cheong, D. Y. T. Pong, A. K. L. Yip, and T. G. F. Li, An extension of Gmumu: General-relativistic resistive magnetohydrodynamics based on staggered-meshed constrained transport with elliptic cleaning, *Astrophys. J. Suppl. Ser.* **261**, 22 (2022).
- [55] P. C.-K. Cheong, H. H.-Y. Ng, A. T.-L. Lam, and T. G. F. Li, General-relativistic radiation transport scheme in Gmumu. I: Implementation of two-moment-based multifrequency radiative transfer and code tests, *Astrophys. J. Suppl. Ser.* **267**, 38 (2023).
- [56] H. Ho-Yin Ng, P. C.-K. Cheong, A. Tsz-Lok Lam, and T. G. F. Li, General-relativistic radiation transport scheme in Gmumu II: Implementation of novel microphysical library for neutrino radiation—Weakhub, *Astrophys. J. Suppl. Ser.* **272**, 9 (2024).
- [57] A. Harten, P. Lax, and B. Leer, On upstream differencing and godunov-type schemes for hyperbolic conservation laws, *SIAM Rev.* **25**, 35 (1983).
- [58] P. Colella and P. R. Woodward, The piecewise parabolic method (PPM) for gas-dynamical simulations, *J. Comput. Phys.* **54**, 174 (1984).
- [59] C.-W. Shu and S. Osher, Efficient implementation of essentially non-oscillatory shock-capturing schemes, *J. Comput. Phys.* **77**, 439 (1988).
- [60] L. R. Weih, E. R. Most, and L. Rezzolla, On the stability and maximum mass of differentially rotating relativistic stars, *Mon. Not. R. Astron. Soc.* **473**, L126 (2018).
- [61] P. L. Espino, V. Paschalidis, T. W. Baumgarte, and S. L. Shapiro, Dynamical stability of quasitoroidal differentially rotating neutron stars, *Phys. Rev. D* **100**, 043014 (2019).
- [62] SpEC: Spectral Einstein code, <https://www.black-holes.org/code/SpEC.html> (Accessed February 27, 2024).
- [63] J. Jesse, M. D. Duez, F. Foucart, M. Haddadi, A. L. Knight, C. L. Cadenhead, F. Hébert, L. E. Kidder, H. P. Pfeiffer, and M. A. Scheel, Axisymmetric hydrodynamics in numerical relativity using a multipatch method, *Classical Quantum Gravity* **37**, 235010 (2020).
- [64] K. N. Gourgouliatos and S. S. Komissarov, Relativistic centrifugal instability, *Mon. Not. R. Astron. Soc.* **475**, L125 (2018).
- [65] M. J. Turk, B. D. Smith, J. S. Oishi, S. Skory, S. W. Skillman, T. Abel, and M. L. Norman, YT: A multi-code analysis toolkit for astrophysical simulation data, *Astrophys. J. Suppl. Ser.* **192**, 9 (2011).
- [66] C. R. Harris *et al.*, Array programming with NumPy, *Nature (London)* **585**, 357 (2020).
- [67] T. Pandas Development Team, pandas-dev/pandas: PANDAS (2020), <https://zenodo.org/records/10957263>.
- [68] Wes McKinney, Data structures for statistical computing in Python, in *Proceedings of the 9th Python in Science Conference*, edited by Stéfan van der Walt and Jarrod Millman (2010), pp. 56–61, <http://conference.scipy.org/.s3-website-us-east-1.amazonaws.com/proceedings/scipy2010/mckinney.html>.
- [69] P. Virtanen *et al.* (SciPy 1.0 Contributors), SciPy 1.0: Fundamental algorithms for scientific computing in Python, *Nat. Methods* **17**, 261 (2020).
- [70] J. D. Hunter, Matplotlib: A 2D graphics environment, *Comput. Sci. Eng.* **9**, 90 (2007).
- [71] T. A. Caswell *et al.*, Matplotlib/Matplotlib: Rel: v3.7.1, <https://zenodo.org/records/7697899> (2023).